Analytical Methods

Accepted Manuscript

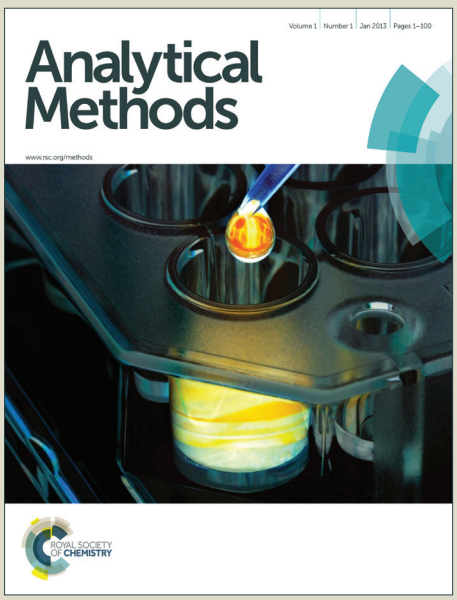

ROYAL SOCIETY OF CHEMISTRY

www.rsc.org/methods

Attenuation of interferences in collision/reaction cell inductively coupled plasma mass spectrometry, using helium and hydrogen as cell gases – Application to multi-element analysis of mastic gum

Nikolaos I. Rousis, Ioannis N. Pasias, Nikolaos S. Thomaidis*

Laboratory of Analytical Chemistry, Department of Chemistry, National and Kapodistrian University of Athens, Panepistimiopolis Zografou, 15771 Athens, Greece

*Corresponding author:

Tel: +30 210 7274317; Fax: +30 210 7274750

E-mail address: ntho@chem.uoa.gr

For submission to: **Analytical Methods**

***Supplementary material**

ABSTRACT

A collision/reaction cell ICP–MS was used to develop a method for the multi-element determination of Na, Mg, Al, K, Ca, Ti, V, Cr, Mn, Fe, Co, Ni, Cu, Zn, As, Se, Sr, Nb, Mo, Ag, Cd, Sb, Cs, Ba, Hg and Pb in mastic gum. Evaluation of helium and hydrogen as cell gases took place and their ability to reduce several interferences arising from Si, S, P, C, Cl and F based matrix was investigated. Likewise, much polyatomic interference was attenuated efficiently by the effect of kinetic energy discrimination. Moreover, a study of stopping curves measurements was performed. Thus, measurements of the ion loss caused by collisions, reaction cross sections given by the Langevin – Gioumousis – Stevenson model and collision cross sections were carried out. The method was validated and the calculated recoveries for all elements (at three concentration levels) were ranged between 92.6% (Ti) – 105% (Ag) and the relative standard deviation (%RSD) of reproducibility was ranged between 1.6% (Co) – 9.9% (Ca). The limits of detection ranged between 0.11 ng g^{-1} (Cs) – 1.12 μg g^{-1} (Ca). The trueness of the method was also checked by the analysis of a standard reference material (SRM, 1573a tomato leaves).

Introduction

Inductively coupled plasma mass spectrometry (ICP–MS) is a widely used technique, because it offers multi – element capability in short time, low detection limits (compared to other atomic spectrometric techniques), large dynamic range, high accuracy and robustness, plus it is able to determine rare earth elements, with sufficient sensitivity.[1-5] Also ICP–MS has the ability to couple with separation techniques (*e.g.* gas chromatography,[6-7] ion chromatography,[8] high performance liquid chromatography,[9] size exclusion chromatography,[10] capillary electrophoresis[11]) and alternative introduction techniques (*e.g.* laser ablation,[12] flow injection analyzers,[13] electrothermal vaporizers[14-15]). Thus, it is applied for trace element determination in biological,[16] geological,[17] pharmaceutical[18] and environmental[19-20] samples, semiconductors,[21] and many more.

Despite all its benefits, there are some limitations, such as spectroscopic and non – spectroscopic interferences. The sources of spectroscopic interferences are isobaric overlap from a second element at the same nominal mass, doubly charged ions, oxides, hydroxides and polyatomic species (**Table S1**).[1-4, 22-33] Many efforts have been made to attenuate these interferences. Mathematical correction equations,[27] high – resolution instruments,[34] collision cells,[35] reaction cells,[36] choice of an alternative isotope,[28,34] cool/cold plasma technology,[37] collision/reaction interface[38] are some approaches to attain the attenuation.

A range of gases are used in collision and reaction cells for the reduction of interferences. Iglesias *et al.*[3] investigated the use of He, H_2, NH_3, N_2O and combinations of He and H_2 to decrease the signal of ArO^+ and improve the detection limit of Fe. Leonhard *et al.*[26] compared the behavior of He and H_2 to minimize ClO^+, ArC^+, $MgCl^+$, $ArNa^+$, $ArMg^+$ and $ArCl^+$ polyatomic interferences. McCurdy and Woods[23] studied S-based polyatomic ions (combinations of S, O, Ar and H) and evaluated the capability of He cell gas to remove these interferences. A list of applications is given by Koppenaal *et al.*[22] and covers the 2000-2003 period. Furthermore to the attenuation that can be obtained by the gas, kinetic energy discrimination (KED) barrier

potential can be established between the cell and the mass analyzer to provide extra attenuation of polyatomic species. Polyatomic ions have larger collision cross sections than analyte ions, so collide more frequently with the cell gas and this causes greater loss of kinetic energy. Consequently, the lower energy ions cannot skip the potential barrier, so they are not able to pass to the mass analyzer.[4, 22, 23, 25, 39-42]

PistaciaLentiscus var. Chia produces a commercially exploitable quantity and quality of resin (mastic) and growths only on the southern part of the Aegean island of Chios. For the above reasons, the mastic has been distinguished and officially retains now as a Protected Designation of Origin product, according to the regulations of the European Union. In just the past few years the Chios Mastiha Growers Association has succeeded in restoring the image of mastic as healthful and in associating its unusual properties with wellness. In keeping with the popularity of aromatherapy, the scent of mastic is now available in soaps, creams, and other cosmetic products.[43] Finally, its antimicrobial, antibacterial and anticancer activity and its positive activity in diseases of teeth, stomach, heart, liver and atherosclerosis are reported.[43-48]

The aim of the present work was to study the interferences in an inductively coupled plasma mass spectrometer with collision/reaction cell (CRC−ICP−MS) system and to develop and validate a method for the multi-element determination of Na, Mg, Al, K, Ca, Ti, V, Cr, Mn, Fe, Co, Ni, Cu, Zn, As, Se, Sr, Nb, Mo, Ag, Cd, Sb, Cs, Ba, Hg and Pb, in mastic samples. Initially an experimental design was applied to optimize the parameters of the digestion procedure in mastic sample. Moreover, the study included optimization of the CRC−ICP−MS parameters and the use of different gases for the attenuation of the interferences. The method was validated and applied in real mastic samples purchased from the Greek market.

Experimental

Instrumentation

An Agilent Technologies 7700x ICP–MS system, which utilizes an octopole ion guide enclosed in a collision/reaction cell, was used throughout. The sample solutions were pumped by peristaltic pump from tubes arranged on an Agilent ASX 500 auto-sampler. A Glass Expansion OpalMist nebulizer and a Savillex, inert sample introduction kit, 2.5 mm ID, cooled to 2°C was used. The interface cones were made of platinum (Pt, Savillex).Argon (Ar), helium (He) and hydrogen (H_2) gases used in the experiment were five-grade (99.999%). **Table 1** summarizes the operating conditions. The ICP instrument parameters were tuned daily under three different conditions as recommended by the manufacturer, in order to achieve the best compromised values for the elements intensities, the oxides and the doubly charged ions. The tuning solution was used to maximize the intensities of ^{7}Li, ^{89}Y and ^{205}Tl in "no gas" mode, ^{59}Co in He mode and ^{59}Y in H_2 mode and to minimize the oxide levels ($CeO^+/Ce^+ < 3\%$) and doubly charged ions ($Ba^{2+}/Ba^+ < 5\%$).

The mastic samples were digested with MARS X microwave oven (CEM Corporation), equipped with a rotor for 12 type ESP 1500 Plus vessels. The optimum values of all variables for the digestion of mastic gum are shown in **Table S4**. A thorough and detailed optimization of the sample digestion procedure was performed in order to achieve complete decomposition of this challenging matrix and the results and discussion can be found in the Electronic Supplementary Information File **(Tables S2 and S3, Figs. S1 to S4).**

Reagents and standards

All solutions were prepared with analytical reagent grade chemicals and ultra pure water (18 MΩ cm) was obtained from a Barnstead, EASYpure®II system. Single element standard stock solutions of 10 µg mL^{-1} Si, P, S, Na, Mg, Al, K, Ca, Ti, V, Cr, Mn, Fe, Co, Ni, Cu, Zn, As, Se, Sr, Nb, Mo, Ag, Cd, Sb, Cs, Ba, Hg and Pb in 2% HNO_3 (High – Purity Standards, Agilent Technologies) were used throughout this study. Also a multi – element internal standard of 100 mg L^{-1} Bi, Ce, In, Li, Lu, Rh, Sc and Tb in 10% HNO_3 (Agilent Technologies) was used. A Certified Reference Material (CRM) from National Institute of

Standards and Technology (NIST), namely tomato leaves (SRM 1573a) was supplied. Nitric acid (HNO_3, 69%, TMA, Hiperpur) and hydrochloric acid (HCl, 35%, TMA, Hiperpur) were purchased from Panreac, whereas hydrofluoric acid (HF, 40%, Suprapur) and n-butanol were obtained from Merck. 500 µg L^{-1} of Sc, Ge, Rh, In and Bi were used as internal standards for the determination of Na-Mg-Al-K-Cr-V-Co-Ni-Ca-Ti-Mn-Fe, Cu-Zn-As-Se-Sr, Nb-Mo, Ag-Cs-Cd-Sb-Ba and Hg-Pb, respectively.

Results and discussion

An effort was made to simulate the elemental mastic matrix in solution and therefore to create the potentially polyatomic interferences in plasma. For this reason, a solution containing 20% (v/v) HCl, 10% (v/v) HNO_3, 10% (v/v) HF, 2% (v/v) S, 2% (v/v) Si, 1% (v/v) P, 5% (v/v) Ca, 5% (v/v) Na and 2% (v/v) n-butanol (as a source of carbon) was considered as blank and used throughout this work for the interferences study. Moreover, a standard solution containing 10 µg L^{-1} for all analytes was used.

Optimization of He and H_2 flow rates

Initially, optimization of He and H_2 flow rates was obtained with both kinetic energy discrimination (w. KED) and without kinetic energy discrimination (w/o. KED). The octopole bias was set at -18 V and the quadrupole bias was set at -15 V when the KED was applied (KED = V_Q - V_O = +3 V) and -21 V when the KED was not applied (KED = V_Q - V_O = -3 V). Both gases were tested for all analytes, except for Cd, Hg and Pb, which are usually determined by “no gas” mode, because of the lack of interferences. Moreover two isotopes were investigated for Ca, Cr, Fe, Cu and Se. The He flow rate was increased in steps of 0.6 mL min^{-1} and the H_2 flow rate was increased in steps of 0.5 mL min^{-1}.

The evaluation of the gas flow rate was done by two criteria. The signal to noise ratio (S/N) is the first one, where S is the intensity (counts s^{-1}) of the 10

μg L^{-1} solution and N is the intensity (counts s^{-1}) of the blank solution. The second is the background equivalent concentration (BEC), which is defined as the apparent concentration of the background signal based on the sensitivity of the element at a specified mass. The lower the BEC value, the more easily a signal generated by an element can be discerned from the background. BEC was estimated as:

$$\text{BEC } (\mu g\ L^{-1}) = [N/(S - N)] \times C_{an} \qquad \text{(eq. 1)}$$

where C_{an} is 10 μg L^{-1}.

For example, when the KED was applied, the intensity of ^{53}Cr has initially increased and then, as the He flow rate was increased, the intensity was decreased, whereas the intensity of the blank solution was reduced from the beginning and was totally diminished at a 4.2 mL min^{-1} flow rate. When KED was not applied, the separation of analyte and its interferences was impossible at low flow rates and when the separation was done attainable, the signal intensity of ^{53}Cr was very low, due to the increased collisions with He (**Fig. 1**).

The slight increase of ^{53}Cr signal at low flow rates can be explained by a mechanism known as “collisional focusing”. As the gas enters the cell, the pressure is getting higher, the energetic distribution of ions is reduced and the ions migrate to the axis of the octopole and this result to a better transmission to the mass analyzer. The signal increase remains until the kinetic energy of the ions gets lower than KED and/or the collisional losses dominate. This mechanism is not so intense in this study on account of the small size of octopole.[4]

The optimum range of gas flow rate was derived from the figures of S/N and BEC *versus* He flow rate. **Fig. 2** shows that the S/N ratio was remained constant in different He flow rates (case w. KED) with higher value at 4.2 mL min^{-1}. Although the S/N value at 2.4 mL min^{-1} was lower, the intensity of ^{53}Cr was four times higher (33,000 cps) compared with the intensity (8,000 cps) at 4.2 mL min^{-1}. Also the blank solution at 2.4 mL min^{-1} had a very small intensity (65 cps) which did not affect the results. Consequently, the range 2.4 – 4.2

mL min^{-1} considered as suitable for ^{53}Cr determination. On the other hand, in case of "w/o. KED" the ratio S/N was very low with an optimum value at 5.4 mL min^{-1} which corresponded to a sensitivity of 114 cps for ^{53}Cr. Furthermore the BEC value was calculated 0.088 μg L^{-1} at 5.4 mL min^{-1} (w/o. KED) and 0.0025 μg L^{-1} at 4.2 mL min^{-1} (w. KED). From the discussion above, the determination of Cr in trace levels can be done using only KED chemistry.

The results for the rest analytes are shown in **Table 2** for He and in **Table 3** for H_2 and the figures can be found in the supplementary file (**Fig. S5 and S6**). The useful range of gas flow rate is represented because compromises between the analytes always apply to a multi – element analysis. The chosen optimum value of the gas always provided a high analyte signal intensity, low BEC and high S/N values. The outcomes of KED chemistry were not so strong for Cs, Mo, As and Mn, for both gases. Ba and Sb showed slightly better results with the use of KED, but only in He mode. The separation of Ag, Nb, Sr, Zn, V, Ti and Al from their interferences were better achieved when the KED was applied, for both gases. Co and Ni were not affected significantly by the application of KED. Generally, the beneficial effect of KED was emphasized and in some cases (Al, Ti, V and Cr in H_2 mode) the determination was not possible without the use of KED.

Stopping curves – Collision cross section – Reaction cross section

Keeping constant the octopole bias at -18 V, we altered the quadrupole bias into a wide range, resulting to "stopping curves" for analytes and interferences (**Fig. 3**). The ions energy can be defined as the quadrupole bias required reducing ions intensity by one order of magnitude. At 0 mL $min^{-1}$of He, the intensity of $^{53}Cr^{+}$ was reduced by one order of magnitude when the quadrupole bias was increased to 3.7 V, which indicates that, the energy with which the ions enter the cell was 21.7 eV. At 2.5 mL min^{-1} the intensity of $^{53}Cr^{+}$ was reduced by one order of magnitude when the quadrupole bias was set to -5.7 V and at 4.5 mL min^{-1} when the quadrupole bias was set to -8.8 V. The difference between the potentials of the quadrupole with He and without He are respectively 9.4 and 12.5 V, which is equivalent to the amount of

energy loss due to collisions with helium. Thus, as the ions pass through the octopole, the kinetic energy is reduced from 21.7 to 12.3 eV and 9.2 eV, respectively.

The same stopping curve measurements were performed for interferences (**Fig. 3**). At 0 mL min^{-1} of He, the interferences intensity (*m/z*=53) was reduced by one order of magnitude when the quadrupole bias was increased to 3.0 V, which indicates that, the energy with which the ions enter the cell was 21.0 eV. At 2.5 mL min^{-1} the interferences intensity was reduced by one order of magnitude when the quadrupole bias was set to -8.2 V and at 4.5 mL min^{-1} when the quadrupole bias was set to -10.8 V. The difference between the potentials of the quadrupole with and without He are respectively 11.2 and 13.8 V, which is equivalent to the amount of energy loss due to collisions with helium. Thus, as the ions pass through the octopole, the kinetic energy is reduced from 21.0 to 9.8 eV and 7.2 eV, respectively.

The above results show that the number of collisions is higher for the polyatomic ions than in monatomic ions, because of the higher cross section of the collision of polyatomic ions, resulting in the smaller kinetic energy in the exit of the cell. This is why with the use of KED the polyatomic ion intensities are reduced more than monatomic ion intensities. The collision cross sections are calculated from the energies of ions before and after the collisions. For the estimation of ions collision cross sections the drag model was applied.[5, 25, 49] The energy losses of ions in the collision cell are fit to:

$$E_{out}/E_{in} = \exp\left[-C_D(m_2/m_1)\sigma n l\right] \qquad \text{(eq.2)}$$

$$\ln(E_{out}/E_{in}) = -C_D(m_2/m_1)\sigma n l \qquad \text{(eq. 3)}$$

where E_{in} is the energy with which an ion enters the cell, E_{out} the exit energy, n the gas number density in the cell, σ the collision cross section, l the cell length, m_1 the ion mass, m_2 the collision gas mass and c_D is the drag coefficient relates the force on an object moving through a gas to the cross sectional area or projection area.

Assuming that the cell gas flows out effusively through the apertures of the cell, n is calculated from the following equation:

$$F = (1/4)\, n\, u\, A \qquad \text{(eq. 4)}$$

where F is the number of gas molecules admitted into the cell per unit time, u is the mean gas velocity and A is the total area of both gas exits. In general, c_D, depends on Reynolds number, Knudsen number and the ratio of the object speed to the thermal speed of the gas.

Consequently, for the same instrument, under the same conditions and for stable cell gas flows rate, the parameters m_2, c_D, n and l from equation 3 remain steady. So, the equation which combines collision cross sections of two (A and B) different ions arise from the division of equations 5A and 5B:

$$\ln(E_{out,A}/E_{in,A}) = -C_D(m_2/m_A)\sigma_A n l \qquad \text{(eq. 5A)}$$

$$\ln(E_{out,B}/E_{in,B}) = -C_D(m_2/m_B)\sigma_B n l \qquad \text{(eq. 5B)}$$

$$\rightarrow \sigma_A/\sigma_B = [m_A \times \ln(E_{out,A}/E_{in,A})]/[m_B \times \ln(E_{out,B}/E_{in,B})] \quad \text{(eq. 6)}$$

and the equation which combines the collision cross sections of two different ions are given by equation 6 (where B is the collision cross section of Ni).

Tables S5 and **S6** summarize the stopping curve results for the analytes and their interferences, which are the entrance energy, the energy loss, the exit energy and the ratio of the ions collision cross section to the collision cross section of Ni and its interferences. The initial kinetic energy of the ions increases with increasing mass.[50] Furthermore among ions of the same mass (analytes and their interferences) a slightly smaller initial energy for the interferences is observed, as a result of the way they formed and the path that they follow until the cell (**Fig. 4**). Moreover, **Fig. 5** shows the correlation between σ_X/σ_{Ni} and *m/z* for He and H_2 in different flow rates. As it is observed the ratio σ_X/σ_{Ni}, did not increase linearly with increasing ratio *m/z*, because the cross-section depends on the size of the ion and not on the mass.

In addition, hydrogen reacts with the ions in the cell and the cross section of the ions depends on the kind and the number of reactions. So the reaction cross section was investigated as a function of the center of mass collision energy and was calculated by the Langevin – Gioumousis – Stevenson (LGS)

model. The reaction cross section (ref. 25 and the references therein), σ_{LGS}, based on (LGS) model, is given from the following equation:

$$\sigma_{LGS} = \pi e(2a/E_{cm})^{1/2} \quad \text{(eq. 7)}$$

where *a* is the polarizability of the H_2 molecule (ca. 0.8×10^{-24} cm^3) and E_{cm} the center of mass collision energy. E_{cm} is estimated from:

$$E_{cm} = E_{in} [m_2/(m_1+m_2)] \quad \text{(eq. 8)}$$

Fig. 6 shows that the reaction cross section (σ_{LGS}), for analytes and interferences, is high at high *m/z*, while the center of mass collision energy (E_{cm}) is low. For low *m/z*ratios, the reversal statements are true.

Gas and isotope selection

For multi elemental analysis, a compromise of the optimum gas flow rates of each element should be done in order to reduce the analysis time. For this reason ^{23}Na, ^{27}Al, ^{24}Mg, ^{39}K, ^{53}Cr, ^{51}V,^{59}Co, ^{60}Ni, ^{65}Cu, ^{66}Zn, ^{75}As,^{93}Nb and ^{95}Mo were determined using He at 4.2 mL min^{-1}, ^{42}Ca, ^{47}Ti, ^{55}Mn, ^{56}Fe,^{78}Se, ^{88}Sr, ^{107}Ag, and ^{133}Cs using H_2 at 3.5 mL min^{-1} and ^{111}Cd, ^{121}Sb, ^{137}Ba,^{202}Hg and $^{206\text{-}208}Pb$ by “no gas” mode.The background signals at m/z 137 and 121 (Ba and Sb) were not decreased with the use of H_2, but He showed good attenuation. During the validation procedure the results between the helium mode and “no gas” mode were similar, but the sensitivity in “no gas” mode was about four times higher, which provides lower limits of detection for these elements. For this reason, Ba and Sb were determined by “no gas” mode. The signals of Cs, Ag, Sr and Mn were kept constant with the increase of hydrogen flow rate and the signals of theirs interferences were too low or/and decreased with the increase of H_2. The signal of Nb in He mode remained very high and it was not reduced with the increase of He flow rate; the interferences did not give any signal, in contrast with the H_2 mode where the interferences produced asignal. Better results were obtained by the use of He gas for the determination of Mo, As, Zn, V, Co, Ni, Al and Mg. The interferences signal of As, Zn, Ni, Co and Mg were too low when He flow rate

was above 4 mL min^{-1} and the signals of these elements were reduced at high flow rates but remained at high values.This was not observed for Co and Ni, where their signals started decreasing at 5.5 mL min^{-1} of He. The signals of V and Al were reduced approximately two orders of magnitude with the use of He at 4.2 mL min^{-1}, but they were remained at high levels, while the signals of their interferences were decreased at extremely low levels.

For Se, the choise of isotope was very crucial because the ^{80}Se isotope had high BEC values and S/N values were <3.3 (He mode) and slightly higher (3.9) for H_2 mode. For ^{78}Se isotope, the comparison between the two gases showed better results for H_2. In addition, Ca showed much better results with H_2 mode and at ^{42}Ca isotope. The BEC reduced from 0.77 to 0.0020 μg L^{-1}. Moreover better results presented by He mode for ^{53}Cr and ^{65}Cu. Eventually for Fe, the He mode was improper (S/N<3.3 with very high BECs), but the H_2 mode produced better results, especially for the ^{57}Fe isotope. Despite the fact that the ^{57}Fe isotope gave better results during the optimization procedure, the ^{56}Fe isotope was finally chosen, because, during the SRM analysis, the determined value was in good agreement with the certified one.

Method validation

Signal stability

Due to instrumental drift that MS systems show, signal stability experiments were carried out. Over a period of 280 min, all analytes and internal standards were measured at regular intervals and their signal was normalized by the first measurement. The results show that internal standardization was necessary, because of the observed drift. The proposed internal standards considered as suitable, because they show the same trend profile with analytes. The above investigation was performed using a standard solution of known concentration: 200 ng L^{-1} (Nb, Mo, Ag, Sb, Cs, Cd, Co); 300 ng L^{-1} (Hg); 1 μg L^{-1} (V, Pb, As, Se); 5 μg L^{-1} (Ba, Sr, Zn, Cu, Ni, Mn, Cr, Ti); 10 μg L^{-1} (Al, Fe, Na, K, Mg, Ca); 500 μg L^{-1} (internal standards).

Calibration and detectability

In order to investigate the presence of matrix effect, three different procedures were tested for calibration: simple aqueous standard solutions, standard additions and matrix matched solutions. It was observed that the slope of the calibration curve from aqueous solutions was statistically different from those of standard additions and matrix matched, so calibration with matrix matched standards should be applied. The matrix matched calibration curves covered the following ranges: 0, 50, 100, 200, 400 ng L^{-1} (Nb, Mo, Ag, Sb, Cs, Cd, Co, Hg); 0, 0.25, 0.50, 1, 2 µg L^{-1} (V, Pb, As, Se); 0, 5, 10, 15, 20µg L^{-1} (Ba, Sr, Zn, Cu, Ni, Mn, Cr, Ti); 0, 5, 10, 20, 40 µg L^{-1} (Na, K, Al, Fe); 0, 100, 200, 400, 800 µg L^{-1} (Ca, Mg). The correlation coefficients (R^2) were ranged from 0.9992 (Ca, V) to 0.999998 (As).

The limit of detection (LOD) and the limit of quantification (LOQ) of the method were estimated from the matrix matched calibration curve. The LOD was calculated from the equation LOD = $(3.3 \times S_{BL} \times V_{dilution}) / (b \times m)$, where S_{BL} is the standard deviation of ten blank determinations, $V_{dilution}$ is the final volume of dilution, *b* is the slope of the curve and *m* is the weighted mass. The LOQ was calculated from the equation LOQ = $(10 \times S_{BL} \times V_{dilution}) / (b \times m)$ (**Table 4**).

Precision

The intra-day precision was evaluated by six replicates at four concentration levels of a mastic sample and the relative standard deviation ($\%RSD_r$) was ranged between 0.8% (Pb, Sr) – 9.1% (Ca). The inter-day precision was estimated by four replicate analyses of the SRM at two different days and the $\%RSD_R$ was calculated by one way ANOVA (**Table 5**). The precision of the method was considered acceptable.

Trueness

The trueness of the method was evaluated by the analysis of the SRM and by recovery experiments at three different levels. The recovery (%R) was calculated from the following equation:

$$\%R = [(C_{sp.} - C_0) / \Delta C] \times 100$$

where: C_{sp} is the found spiked concentration, C_0 is the concentration of each element in mastic gum and ΔC is the spiked concentration. The calculated recoveries for all elements at three concentration levels (n = 6, each) ranged between 92.6% (Ti) – 105% (Ag).

A student t–test was performed to check the existence of statistical significant difference between the "true" and the found values of the SRM. For a confidence level of 95% and at three degrees of freedom, t_{exp} was lower than t_{theor} (3.182) for all the analytes (**Table 5**), which means that the method is free of systematic errors.

Application

A raw material of mastic gum was analyzed (n = 6) and the results are listed in **Table 5**. To the best of our knowledge, there is only one study[51] for the determination of the elemental content of mastic gum. In general, both studies agree on the determined levels. Some differences that occur cannot be explained because there is a lack of data for this sample type, as well as for the collection period and the processing stage.

Conclusions

A method for the multi-element determination of Na, Mg, Al, K, Ca, Ti, V, Cr, Mn, Fe, Co, Ni, Cu, Zn, As, Se, Sr, Nb, Mo, Ag, Cd, Sb, Cs, Ba, Hg and Pb in mastic gum was developed and validated using an octopole CRC – ICP – MS instrument. A comparative study of helium and hydrogen as cell gases was performed for the majority of elements and their interferences. Gas flow rate optimization with kinetic energy discrimination and without kinetic energy

discrimination was performed. The investigation showed that some elements cannot be detected without the use of KED, or had very high LODs. The beneficial effects of KED were emphasized by the improvement of BEC values and the interferences attenuation. The kinetic energy loss was calculated in two gas flow rate levels and the high one reduced more effectively the polyatomic ions. Figures presenting the collision cross sections demonstrated that the size of ions plays important role and the reaction cross section figures showed that high mass to charge ratios have high σ_{LGS} and low E_{cm} values and low mass to charge ratios have low σ_{LGS} and high E_{cm} values. Moreover, isotope investigation for five elements took place. For Se, the choise of isotope was very crucial because the ^{80}Se isotope had high BEC values and the S/N values were <3.3 (He mode) and slightly higher (3.9) for H_2 mode. For ^{78}Se isotope, the comparison between the two gases showed that H_2 performed better.Likewise, Ca showed better results with H_2 mode and at ^{42}Ca isotope. Additionally, better results produced by He mode for ^{53}Cr and ^{65}Cu. Finally, for Fe, the He mode was inadequate (S/N<3.3 and very high BECs), but the H_2 mode showed good results. Furthermore, the use of H_2 instead of He is suggested for the determination of Ca, Ti, Mn, Fe,Se, Sr, Ag and Cs and “no gas” mode is suggested for the determination of Cd, Sb, Ba, Hg and Pb.

The accuracy of the method was confirmed by the analyses of SRM and the calculated recoveries at three different levels were ranged between 92.6% (Ti) and 105% (Ag). The limits of detections were ranged between 0.11 ng g^{-1} (Cs) – 1.12 μg g^{-1} (Ca). It should be emphasized that matrix matched curves should be used for reliable results. Finally, the method was considered as fit for its purpose for the multi-element determination of 26 elements in Chios mastic gum.

Acknowledgements

The authors would like to thank Dr. Paul Nisianakis, the director of the Analytical Chemistry Laboratory of the Center of Biological Research of Armed Forces (Ministry of National Defense) for the provision of the CRC –

ICP – MS instrument. This research was partially funded by the University of Athens, Special Account of Research Grants, no 10812.

References

1. K.L.Linge and K. E. Jarvis, *Geostand. Geoanal. Res.*, 2009, **33(4)**, 445-467.
2. A. Kadar, L. Noel, R. Chekri, C. Vastel, S. Millour and T. Guerin,*Talanta*, 2011, **85**, 2605-2613.
3. M. Iglesias, N. Gilon, E. Poussel and J-M. Mermet, *J. Anal. At. Spectrom.*, 2002, **17**, 1240-1247.
4. A.J. B. Cotta and J. Enzweiler, *J. Anal. At. Spectrom.*, 2009, **24**, 1406-1413.
5. Z. Du and R.S. Houk, *J. Anal. At. Spectrom.*, 2000, **15**, 383-388.
6. J.C.A. Wuilloud, R.G. Wuilloud, A.P. Vonderheide and J.A. Caruso, *Spectrochim. Acta Part B*, 2004, **59**, 755-792.
7. B. Bouyssiere, J. Szpunar and R. Lobinski, *Spectrochim. Acta Part B*, 2002, **57**, 805-828.
8. Z. Chen, W. Wang, M. Mallavarapu and R. Naidu,*Spectrochim. Acta Part B*, 2008, **63**, 69-75.
9. G. Zhai, J. Liu, L. Li, L. Cui, B. He, Q. Zhou and G. Jiang,*Talanta*, 2009, **77**, 1273–1278.
10. B.A. Lesniewska, J.Messerschmidt, N. Jakubowski and A. Hulanicki, *Sci. Total Environ*., 2004, **322**, 95–108.
11. J.C. Stern, J. E. Sonke and V.J.M. Salters, *Chem. Geol.*, 2007, **246**, 170–180.
12. S. Compernolle, D. Wambeke, I. de Raedt and F. Vanhaecke, *Spectrochim. Acta Part B*, 2012, **67**, 50–56.
13. F.R.S. Bentlin, C.M. M. dos Santos, E.M. M. Flores and D. Pozebon, *Anal. Chim. Acta*, 2012, **710**, 33–39.
14. Y. Zhang and B. Hu, *Spectrochim. Acta Part B*, 2011, **66**, 163–169.
15. M. Aramendia, M. Resano and F. Vanhaecke, *Anal. Chim. Acta*, 2009, **648**, 23–44.
16. J. Gomez-Espina, E. Blanco-Gonzalez, M. Montes-Bayon and A. Sanz-Medel,*J. Anal. At. Spectrom.*, 2012, **27**, 1949-1954.
17. W. Zhang, Z. Hu, Y. Liu, L. Chen, H. Chen, M. Li, L. Zhao, S. Hu and S. Gao, *Geostand. Geoanal. Res.*, 2012, **36**, 271-289.

18. A.L.H. Muller, P.A. Mello, M.F. Mesko, F.A. Duarte, V.L. Dressler, E. I. Muller and E. M.M. Flores,*J. Anal. At. Spectrom*., 2012, **27**, 1889-1894.
19. D. Beauchemin, *Mass Spectrom. Rev*., 2010, **29**, 560–592.
20. M.L.A. Castillo, A.G. de Torres, E.V. Alonso, M.T.S. Cordero and J.M.C. Pavón, *Talanta*, 2012, **99**, 853–858.
21. J.S. Becker and H.J. Dietze, *Int. J. Mass Spectrom*., 2000, **197**, 1-35.
22. D.W. Koppenaal, G. C. Eiden and C.J. Barinaga, *J. Anal. At. Spectrom.*, 2004, **19**, 561-570.
23. E. McCurdy and G. Woods, *J. Anal. At. Spectrom*. 2004, **19**, 607-615.
24. H. Yuan, S. Hu, J. Tong, L. Zhao, S. Lin and S. Gao, *Talanta*, 2000, **5**, 971-981.
25. N. Yamada, J. Takahashi and K. Sakata, *J. Anal. At. Spectrom*., 2002, **17**, 1213-1222.
26. P. Leonhard, R. Pepelnik, A. Prange, N. Yamada and T. Yamada, *J. Anal. At. Spectrom.*, 2002, **17**, 189-196.
27. D. Pick, M. Leiterer and J.W. Einax, *Microchem. J*., 2010, **95**, 315-319.
28. D. Muynck and F. Vanhaecke, *Spectrochim. Acta Part B*, 2009, **64**, 408-415.
29. A. S. Gonzalez, J. M. M. Gayon, J. M. T. Lobo, J. P. Jimenez and A. S. Medel, *Anal. Bioanal. Chem*., 2005, **382**, 1001-1009.
30. S.F. Boulyga, H.J. Dietze and J.S. Becker, *Microchim. Acta*, 2001, **137**, 93-103.
31. C. Agatemor and D. Beauchemin, *Spectrochim. Acta Part B*, 2011, **66**, 1-11.
32. W. Guo, S. Hu, J. Zhao, S. Jin, W. Liu and H. Zhang, *Microchem. J*., 2011, **97**, 154–159.
33. F. Vanhaecke and L. Moens, *Anal. Bioanal. Chem*. 2004, **378**, 232–240.
34. S.Y. Ng, A. Zou, L.P. Sim, Y. Ding, K.L. Yuen, R.Y. C. Shin and T.K. Lee, *Int. J. Mass Spectrom*., 2012, **321–322**, 19–24.
35. V. Dufailly, L. Noël and T. Guérin, *Anal. Chim. Acta*, 2008, **611**, 134–142.
36. F.I. de Albuquerque, C.B. Duyck, T.C.O. Fonseca and T.D. Saint'Pierre, *Spectrochim. Acta Part B*, 2012, **71-72**, 112–116.

37. L.S. Huang and K.C. Lin, *Spectrochim. Acta Part B*, 2001, **56**,123-128.
38. R.F.S. Salazar, M.B.B. Guerra, E. R. Pereira-Filho and J.A. Nóbrega,*Talanta*, 2011, **86**, 241–247.
39. B. Hattendorf and D. Günther, *J. Anal. At. Spectrom.*, 2004, **19**, 600-606.
40. M.A. Dexter, H. J. Reid and B.L. Sharp, *J. Anal. At. Spectrom.*, 2002, **17**, 676-681.
41. V. Chrastný, M. Komárek, M. Mihaljevič and J. Štichová, *Anal. Bioanal. Chem.*, 2006, **385**, 962-970.
42. S. D. Tanner, V. I. Baranov and D. R. Bandura,*Spectrochim. Acta Part B*, 2002, **57**, 1361-1452.
43. P. Freedman, *Mediterr. Hist. Rev.*, 2011, **26**, 99-113.
44. S. Paraschos, P. Magiatis, P. Gousia, V. Economou, H. Sakkas, C. Papadopoulou and A.-L. Skaltsounis,*Food Chem.*, 2011, **129**, 907-911.
45. K. Doi, M. Wei, M. Kitano, N. Uematsu, M. Inoue and H. Wanibuchi, *Toxicol. Appl. Pharmacol.*, 2009, **234**, 135-142.
46. A. Aksoy, N. Duran and F. Koksal, *Arch. Oral Biol.*, 2006, **51**, 476-481.
47. K.J. Dabos, E. Sfika, L.J. Vlatta and D. Frantzi, *J. Ethnopharmacol.*, 2010, **127**, 205-209.
48. G.V.Z. Dedoussis, A.C. Kaliora, S. Psarras, A. Chiou, A. Mylona, N.G. Papadopoulos and N.K. Andrikopoulos, *Atherosclerosis*, 2004, **174**, 293-303.
49. Y.L. Chen, B. A. Collings and D.J. Douglas, *J. Am. Soc. Mass Spectrom.*, 1997, **8**, 681-687.
50. H. Niu and R. S. Houk, *Spectrochim. Acta Part B*,1996, **51**, 779-815.
51. G. A. Zachariadis and E. A. Spanou, *Phytochem. Anal.*, 2011, **22**, 31-35.

Table 1 Instrumental settings of the CRC–ICP–MS

Plasma parameters	
RF Power	1550 W
RF Matching	1.60 V
Sampling Depth	8.0 mm
Carrier Gas	0.99 L min^{-1}
Spray Chamber Temperature	2 °C
Ion lenses parameters	
Extract 1	0 V
Extract 2	−200 V
Omega Bias	−80 V
Omega Lens	7.8 V
Cell Entrance	−40 V
Cell Exit	−60 V
Deflect	1.4 V
Plate Bias	−60 V
Collision/Reaction parameters	
Octopole Bias	−18 V
Octopole RF	200 V
Kinetic Energy Discrimination	+4 V
He Flow Rate	4.2 mL min^{-1}
H_2 Flow Rate	3.5 mL min^{-1}
Correction equations	
$^{115}In^+ = {}^{115}Peak^+ - 0.016\ {}^{118}Peak^+$	
$^{208}Pb^+ = {}^{206}Pb^+ + {}^{207}Pb^+ + {}^{208}Pb^+$	

Table 2 Optimization results of He flow rate for analytes

	with KED				without KED			
	He (mL min^{-1})	S/N	BEC (μg L^{-1})	Range (mL min^{-1})	He (mL min^{-1})	S/N	BEC (μg L^{-1})	Range (mL min^{-1})
^{24}Mg	4.2	11	1.0	2.4−4.2	3.0	7.6	1.5	2.4−3.6
^{27}Al	3.0	146	0.069	1.8−4.2	3.0	1.4	25	2.4−3.6
^{42}Ca	2.4	14	0.77	1.8−3.6	3.6	49	0.21	2.4−4.2
^{43}Ca	3.0	244	0.041	1.8−4.8	3.0	158	0.063	1.8−3.6
^{47}Ti	1.2	1,355	0.0074	0.6−4.2	3.0	4.5	2.8	2.4−3.0
^{51}V	3.0	7,060	0.0014	1.2−4.8	4.2	120	0.083	3.0−4.8
^{52}Cr	4.2	1,670	0.0060	2.4−5.4	3.6	79	0.13	2.4−4.8
^{53}Cr	4.2	4,000	0.0025	2.4−4.8	3.6	21	0.50	3.0−4.2
^{55}Mn	4.2	320	0.031	2.4−4.8	4.2	215	0.047	3.0−5.4
^{56}Fe	3.6	2.5	6.5	2.4−6.0	2.4	2.2	8.1	2.4−4.2
^{57}Fe	3.6	2.8	5.3	1.8−4.8	1.8	5.0	2.5	1.2−4.8
^{59}Co	4.8	660	0.015	2.4−6.0	3.6	140	0.072	2.4−5.4
^{60}Ni	4.8	110	0.091	3.0−6.0	4.2	13	0.84	3.6−6.0
^{63}Cu	4.8	70	0.15	2.4−6.0	4.2	80	0.13	2.4−5.4
^{65}Cu	4.8	75	0.13	2.4−5.4	3.6	75	0.13	3.0−5.4
^{66}Zn	3.6	60	0.17	1.8−4.8	3.0	17	0.62	2.4−3.6
^{75}As	4.2	18	0.60	1.8−4.8	3.6	22	0.49	2.4−4.2
^{78}Se	4.2	20	0.56	2.4−4.8	3.6	15	0.70	3.0−4.2
^{80}Se	5.4	2.4	7.3	4.2−5.4	4.8	1.7	13	3.6−5.4
^{88}Sr	3.6	2,800	0.0036	1.8−4.2	1.8	23	0.45	1.8−3.0
^{93}Nb	2.4	25,00	0.00040	1.8−4.2	3.6	428	0.023	2.4−4.8
^{95}Mo	3.0	1,000	0.0098	1.8−4.2	2.4	640	0.015	1.8−4.2
^{107}Ag	4.2	325	0.031	1.8−4.8	2.4	145	0.069	1.8−3.6
^{121}Sb	2.4	670	0.015	1.2−4.2	2.4	370	0.027	0.0−3.0
^{133}Cs	3.0	1,800	0.0055	1.2−4.2	3.6	1,60	0.0062	2.4−4.2
^{137}Ba	3.0	300	0.033	1.8−4.2	2.4	190	0.053	1.8−4.2
Units: He and Range (mL min^{-1}); BEC (μg L^{-1})								

542 **Table 3** Optimization results of H_2 flow rate for analytes

	with KED				without KED			
	H_2	S/N	BEC	Range	H_2	S/N	BEC	Range
^{24}Mg	4.5	75	0.13	2.0-5.0	5.0	5.4	2.3	3.5-5.0
^{27}Al	4.5	15	0.73	2.0-5.5	-	-	-	-
^{42}Ca	5.0	4,920	0.0020	2.0-6.0	4.0	17	0.64	2.5-5.5
^{43}Ca	4.5	4,000	0.0025	0.5-6.0	2.0	88	0.11	1.5-5.0
^{47}Ti	5.0	51	0.20	3.5-5.0	-	-	-	-
^{51}V	4.5	19	0.55	4.0-5.5	-	-	-	-
^{52}Cr	4.0	142	0.071	2.5-5.0	-	-	-	-
^{53}Cr	4.0	35	0.29	2.5-5.5	-	-	-	-
^{55}Mn	4.5	147	0.068	3.0-6.0	4.5	94	0.11	2.5-6.0
^{56}Fe	4.0	6.5	1.8	3.0-6.0	4.0	4.6	2.8	3.0-6.0
^{57}Fe	4.0	11	1.0	3.0-6.0	4.0	8.7	1.3	3.0-5.0
^{59}Co	5.0	47	0.22	3.0-6.0	5.5	121	0.083	3.0-6.0
^{60}Ni	3.0	36	0.28	2.0-4.5	2.5	36	0.28	1.5-4.0
^{63}Cu	3.0	40	0.26	2.0-4.5	3.0	39	0.27	2.0-4.5
^{65}Cu	3.0	24	0.43	1.5-4.5	3.0	28	0.37	2.0-4.0
^{66}Zn	4.0	116	0.087	1.5-5.0	1.5	13	0.81	0.5-2.0
^{75}As	3.5	6.0	2.0	3.0-5.0	3.5	5.7	2.1	3.0-5.0
^{78}Se	3.0	34	0.30	2.0-5.5	2.5	30	0.34	1.5-5.0
^{80}Se	3.0	3.9	3.5	2.5-5.5	3.5	4.2	3.1	2.5-5.5
^{88}Sr	4.5	1,300	0.0078	1.5-6.0	3.0	34	0.30	1.0-4.5
^{93}Nb	4.0	5,090	0.0019	1.5-5.0	2.5	350	0.029	1.5-3.5
^{95}Mo	2.5	720	0.014	2.0-4.5	3.5	510	0.020	1.5-4.0
^{107}Ag	3.5	1,660	0.0060	1.5-4.5	2.0	86	0.12	1.0-3.5
^{121}Sb	4.5	51	0.20	2.5-6.0	2.5	43	0.24	1.5-5.0
^{133}Cs	3.0	1,000	0.010	1.5-5.0	3.0	1,500	0.0066	1.4-4.5
^{137}Ba	2.5	9.2	1.2	1.5-5.0	2.0	11	1.0	1.0-3.0

Units: H_2 and Range (mL min^{-1}); BEC (μg L^{-1})

543

544

Table 4 Detection limits, quantification limits of investigated elements and the used mode for the attenuation of interferences

	LOD	LOQ	Mode
Na (µg g^{-1})	0.14	0.43	He
Mg (µg g^{-1})	0.54	1.65	He
Al (µg g^{-1})	0.14	0.43	He
K (µg g^{-1})	0.49	1.47	He
Ca (µg g^{-1})	1.12	3.40	H_2
Ti (ng g^{-1})	20.8	62.9	H_2
V (ng g^{-1})	10.6	32.0	He
Cr (ng g^{-1})	8.56	25.9	He
Mn (ng g^{-1})	18.0	54.0	H_2
Fe (µg g^{-1})	0.11	0.32	H_2
Co (ng g^{-1})	0.76	2.30	He
Ni (ng g^{-1})	22.9	69.9	He
Cu (ng g^{-1})	22.4	67.8	He
Zn (ng g^{-1})	74.9	227	He
As (ng g^{-1})	2.72	8.24	He
Se (ng g^{-1})	1.36	4.11	H_2
Sr (ng g^{-1})	29.3	88.9	H_2
Nb (ng g^{-1})	0.19	0.58	He
Mo (ng g^{-1})	1.63	4.94	He
Ag (ng g^{-1})	0.82	2.47	H_2
Cd (ng g^{-1})	1.47	4.44	no gas
Sb(ng g^{-1})	0.57	1.71	no gas
Cs(ng g^{-1})	0.11	0.32	H_2
Ba(ng g^{-1})	14.1	42.5	no gas
Hg(ng g^{-1})	1.20	3.64	no gas
Pb(ng g^{-1})	1.14	3.44	no gas

Table 5 Inter-day precision data, SRM (n = 4×2) and mastic gum (n = 6) results.

	Standard reference material of tomato leaves (1573a)				Mastic gum
	Certified value (μg g^{-1})	Found value (μg g^{-1})	%RSD	$t_{exp.}$	(μg g^{-1})
Na	136	143.0±4.8	4.3	2.703	19.4±1.1
Mg	1.2%	(1.30±0.12)%	7.5	1.635	167.4±6.7
Al	598	530±53	6.6	2.595	23.72±0.92
K	2.7%	(2.596±0.082)%	3.6	2.536	12.46±0.30
Ca	5.05%	(5.038±0.032)%	9.9	0.076	$(0.294\pm0.027)\times10^{3}$
Ti	−	67.4±3.3	4.0	−	2.47±0.15
V	0.835	0.791±0.030	2.9	2.930	0.133±0.012
Cr	1.99	1.78±0.15	6.4	2.770	0.1293±0.0075
Mn	−	237.9±5.8	3.9	−	0.406±0.017
Fe	368	365.5±3.9	5.3	3.182	20.1±1.0
Co	0.57	0.5725±0.0058	1.6	0.741	0.01452±0.0052
Ni	1.59	1.53±0.10	6.8	1.236	0.2133±0.0092
Cu	4.7	4.86±0.24	3.7	1.287	0.471±0.029
Zn	30.9	30.23±0.48	1.7	2.781	1.77±0.12
As	0.112	0.118±0.0057	3.9	1.989	0.0825±0.0072
Se	0.054	0.052±0.0026	6.4	1.827	0.0109±0.0014
Sr	85	83.8±1.8	4.0	1.310	0.480±0.043
Nb	−	0.188±0.010	4.6	−	$(4.33\pm0.21)\times10^{-3}$
Mo	0.46	0.461±0.010	2.6	0.219	‹ LOQ
Ag	−	0.0250±0.0015	5.1	−	$(4.92\pm0.30)\times10^{-3}$
Cd	1.52	1.566±0.029	2.0	3.130	0.0173±0.0011
Sb	0.063	0.0645±0.0064	8.0	0.465	< LOQ
Cs	53	53.5±2.1	3.5	0.515	$(8.12\pm0.54)\times10^{-3}$
Ba	63	61.8±1.5	2.4	1.574	0.3703±0.0059
Hg	0.034	0.03475±0.0091	4.3	1.664	$(8.74\pm0.39)\times10^{-3}$
Pb	−	1.055±0.050	3.9	−	0.2979±0.0024

Figure Legends

Fig.1. Signal intensities of ^{53}Cr and its interferences (blank) as a function of He flow rate: a) w. KED and b) w/o. KED.

Fig.2. Effect of the increase of He flow rate in S/N and BEC for ^{53}Cr.

Fig.3. Stopping curves for ^{53}Cr and its interferences (*m/z*=53). The octopole bias was set at -18 V.

Fig.4. Initial kinetic energy of ions versus mass to charge ratio.

Fig.5. Collision cross sections of ions versus mass to charge ratio; a) He 2.5 mL min^{-1}; b) He 4.5 mL min^{-1}; c) H_2 2.5 mL min^{-1}; d) H_2 4.5 mL min^{-1}.

Fig.6. Reaction cross sections (σ_{LGS}) and center of mass collision energies (E_{cm}) versus mass to charge ratios.

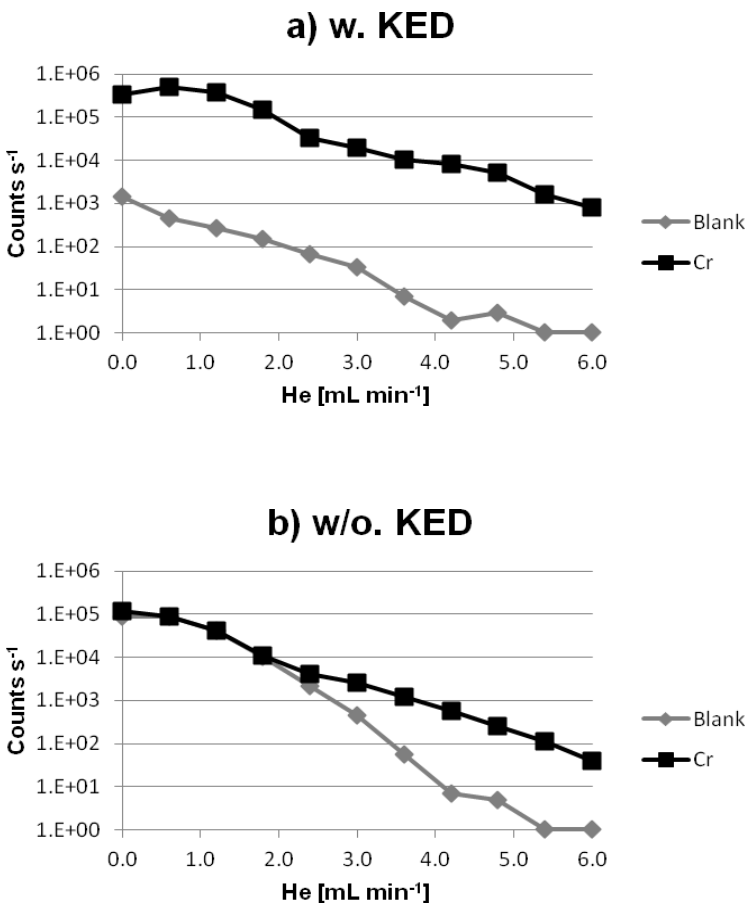

Fig. 1

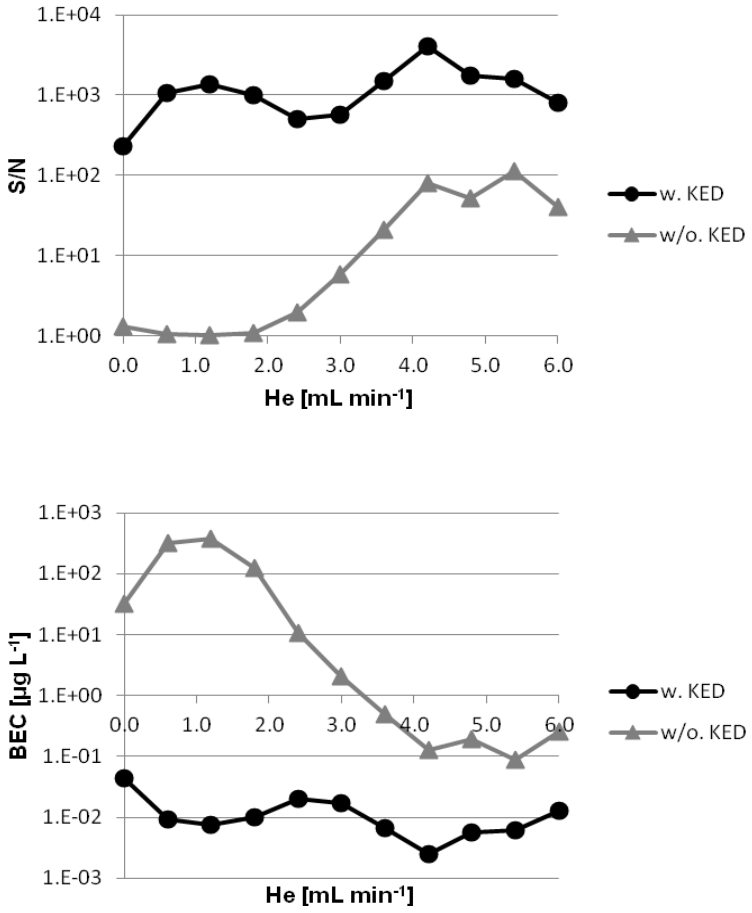

Fig. 2

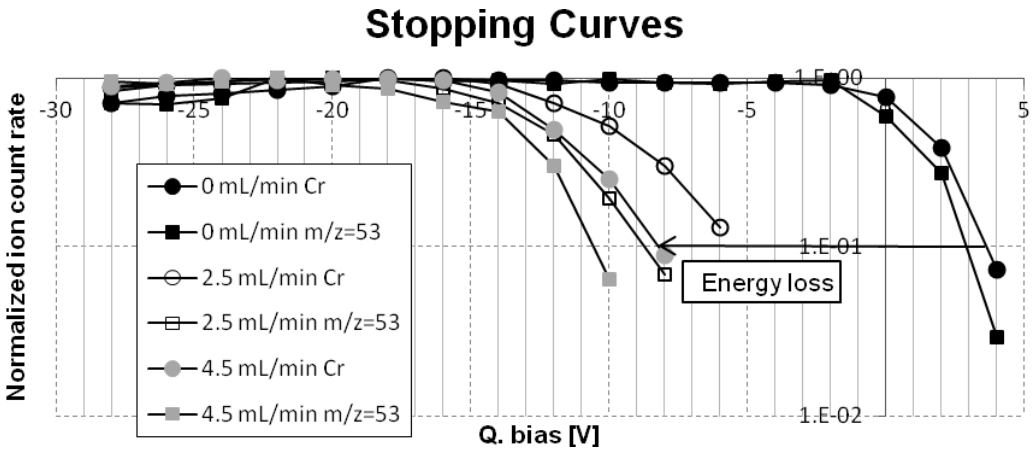

Fig. 3

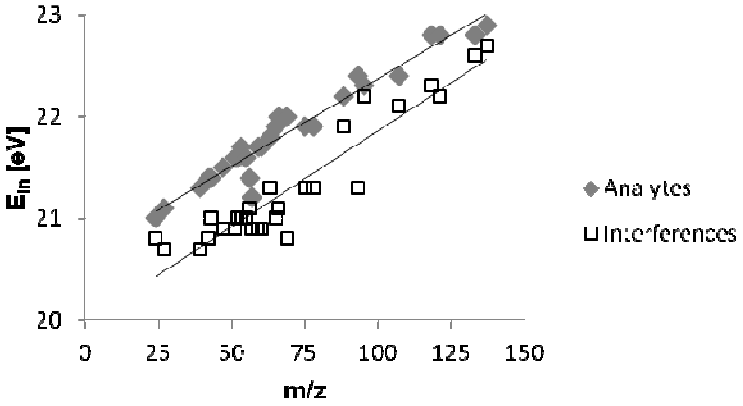

Fig. 4

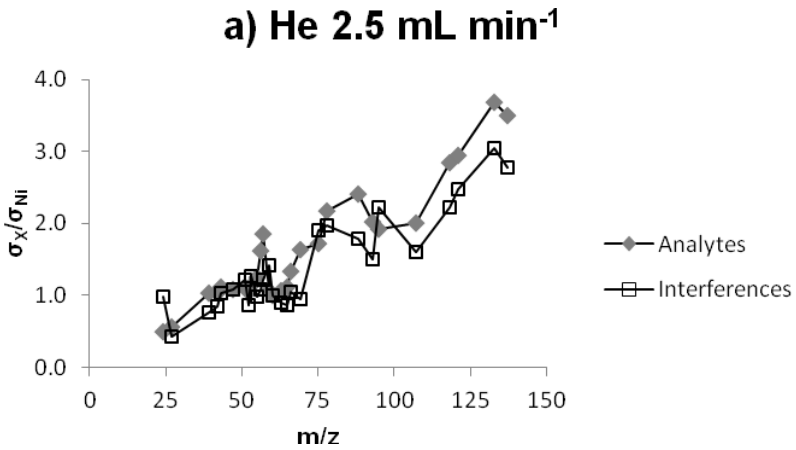

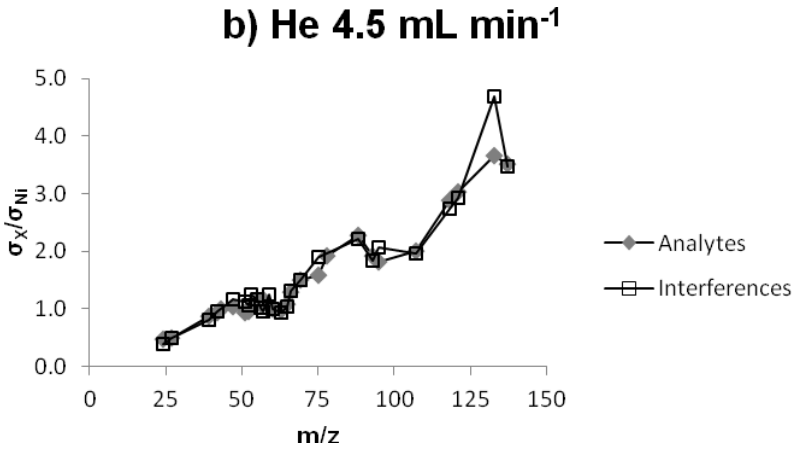

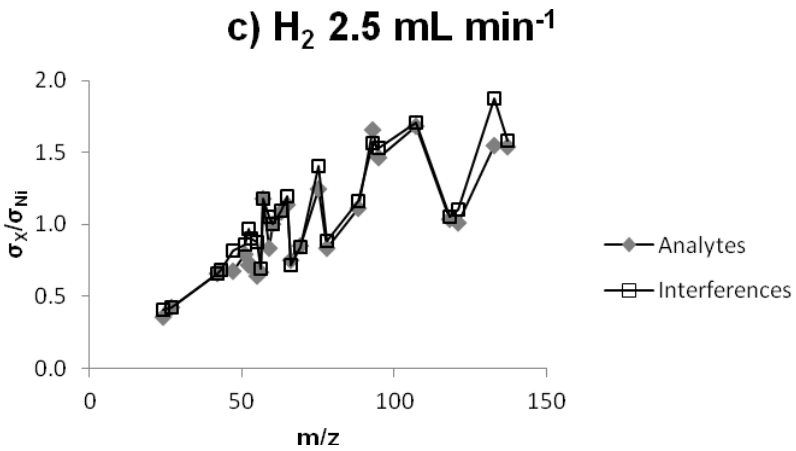

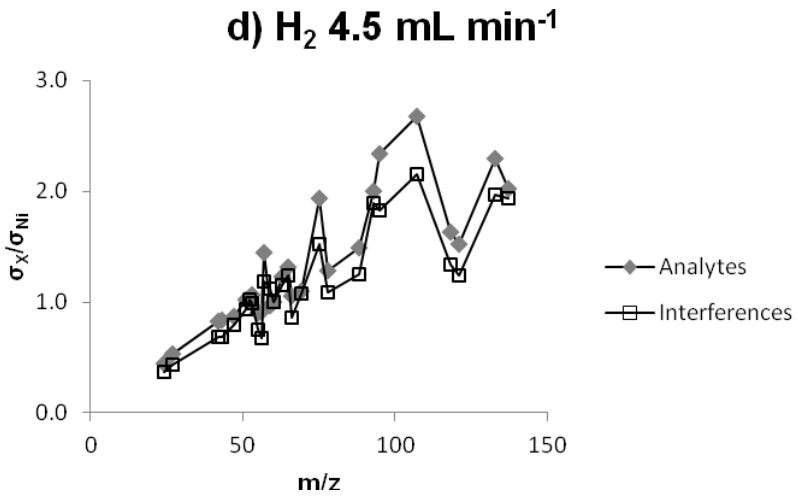

Fig. 5

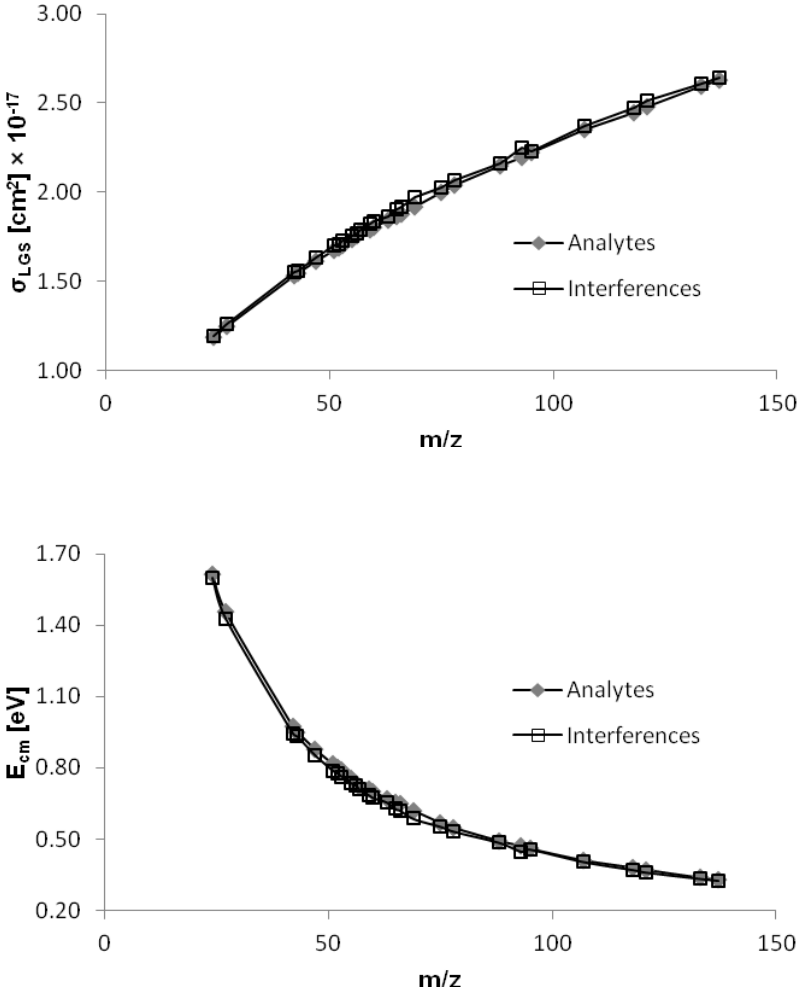

Fig. 6